Phonon focusing in piezoelectric crystals

A. G. Every
Department of Physics, University of the Witwatersrand, Johannesburg 2001, South Africa

A. K. McCurdy
Electrical Engineering Department, Worcester Polytechnic Institute, Worcester, Massachusetts 01609
(Received 29 January 1987)

Striking changes are predicted in acoustic wave propagation and the phonon-focusing properties of piezoelectric crystals as a result of the piezoelectric stiffening of the elastic constants. Phase and group velocities and phonon enhancement factors have been calculated using a general method applicable to crystals of any symmetry. Monte Carlo phonon-focusing patterns are presented for a number of the more strongly piezoelectric crystals on which the required material constants are available. The effects of piezoelectric stiffening are generally only pronounced when one or more of the electromechanical coupling constants exceeds 0.1, but become important at much smaller values of the coupling if the elastic anisotropy is small. An important consequence of piezoelectric stiffening is that the degree of the equation of the slowness surface is raised from 6 to 12. As a result the innermost sheet of this surface need not be entirely convex, and fast phonon-branch focusing caustics are permitted. Rochelle salt and $Ba_2NaNb_5O_{15}$ are two crystals which possess this property.

I. INTRODUCTION

In strongly piezoelectric crystals the coupling between elastic and electric variables has a profound influence on the nature of the acoustic modes and on phonon transport. Through this coupling the strain field accompanying an acoustic wave gives rise to an electric field, and this in turn leads to an enhancement of the stress field. The material thus appears elastically stiffened, and the phase velocity and other characteristics of the wave are modified. It is well known that the effect can be treated by replacing the elastic moduli in the Christoffel wave equations by a set of "stiffened elastic constants" which are functions of the wave normal.[1,2] Account has to be taken of this effect in interpreting ultrasonics data,[1] phonon-focusing patterns,[3] boundary-limited thermal conduction in crystals,[4] ferroelastic mode softening,[5] and other such phenomena in any medium with a sizable piezoelectric effect. In a crystal like $LiNbO_3$, for instance, the relative changes in velocity brought about by piezoelectric stiffening are as large as 28% in some directions.[6] Furthermore, Koos and Wolfe[7] have shown that the phonon-focusing pattern of this crystal is dramatically altered by piezoelectric stiffening. The fast transverse (FT) phonon branch acquires a prominent set of caustics and the caustics of the slow transverse (ST) phonon branch are considerably changed in appearance. Also, the directions of most of the acoustic axes are shifted appreciably.

The aim of this paper is to demonstrate that piezoelectric stiffening is an important consideration in treating phonon focusing in a wide variety of crystals. To this end we describe the changes brought about by piezoelectric stiffening in the phonon-focusing patterns of a number of strongly piezoelectric crystals on which the required data is available. Our examples are drawn from many of the crystal classes, showing that strong piezoelectric influence is a widespread phenomenon and not restricted to any particular crystal symmetry. An important consequence of piezoelectric stiffening, which we report, is that the degree of the equation of the slowness surface is raised from 6 to 12. As a result, the innermost sheet of this surface is allowed to possess negatively curved regions and so fast phonon branch caustics are permitted. Examples of crystals having this property are provided later in this paper.

Our analysis assumes the long-wavelength acoustic limit and is based on continuum elasticity theory incorporating linear electromechanical coupling. We outline a convenient method of solving the stiffened Christoffel equations and calculating phonon group velocities and phonon enhancement factors. Our procedure is quite general and is applicable to crystals of any symmetry class.

II. THE ACOUSTIC WAVE EQUATION IN PIEZOELECTRIC MEDIA

In a piezoelectric medium the electric and elastic variables are coupled, and this has an important effect on the dynamics of the system. The constitutive relations expressing this coupling may be written in the form[1,2]

$$\begin{aligned} \sigma_{ij} &= C^E_{ijlm} S_{lm} - e_{ijr} E_r \ , \\ D_r &= e_{ijr} S_{ij} + \epsilon^S_{rl} E_l \ , \end{aligned} \tag{1}$$

where **E** is the electric field, **D** is the electric displacement vector, σ_{ij} is the elastic stress tensor,

$$S_{lm} = \frac{1}{2}\left[\frac{\partial u_l}{\partial x_m} + \frac{\partial u_m}{\partial x_l}\right] , \tag{2}$$

is the elastic strain, and $\mathbf{u}(x,t)$ is the displacement field of

the medium. These quantities are related through the elastic modulus tensor at constant electric field C^E_{ijlm}, the piezoelectric stress tensor e_{ijr} and the permittivity tensor at constant strain ϵ^S_{rl}. The contracted Voigt notation[8] is used to represent these tensors as matrices C_{IJ}, e_{rI}, and ϵ_{pq}. The forms that these three matrices take for the different crystal classes is shown in Table I, the entries being arranged as follows:

C_{11}	·	·	·	·	C_{16}	e_{11}	·	e_{31}
·	·	·	·	·	·	·	·	·
·	·	·	·	·	·	·	·	·
·	·	·	·	·	·	·	·	·
·	·	·	·	·	·	·	·	·
C_{16}	·	·	·	·	C_{66}	e_{16}	·	e_{36}
e_{11}	·	·	·	·	e_{16}	ϵ_{11}	·	ϵ_{13}
·	·	·	·	·	·	·	·	·
e_{31}	·	·	·	·	e_{36}	ϵ_{13}	·	ϵ_{33}

In the absence of body forces and torques the local force on the medium is given by the stress gradient, and the equations of motion are

$$\rho\frac{\partial^2 u_i}{\partial t^2}=\frac{\partial \sigma_{ij}}{\partial x_j}\ , \tag{3}$$

where ρ is the density of the medium. These equations admit plane wave solutions of the form

$$\mathbf{u}=\mathbf{U}e^{i(\omega t-\mathbf{k}\cdot\mathbf{x})}\ . \tag{4}$$

Acoustic phase velocities $v=\omega/k$ are typically 5 orders of magnitude smaller than the velocity of light c, and so the electric field accompanying an acoustic wave may be treated as quasistatic, i.e., derivable from a scalar potential ϕ, and the magnetic vector potential and induction ignored. Since ϕ must have the phase dependence of $\mathbf{U}$, i.e.,

$$\phi=\phi_0 e^{i(\omega t-\mathbf{k}\cdot\mathbf{x})}\ , \tag{5}$$

it follows that the electric field

$$E_l=(-\nabla\phi)_l=ik_l\phi_0 e^{i(\omega t-\mathbf{k}\cdot\mathbf{x})} \tag{6}$$

is constrained to lie in the direction of $\mathbf{k}$. One further assumes that there are no free charges, so that

TABLE I. Elasto-piezoelectric-dielectric matrices for the 32 crystal classes, adapted from Ref. 9.

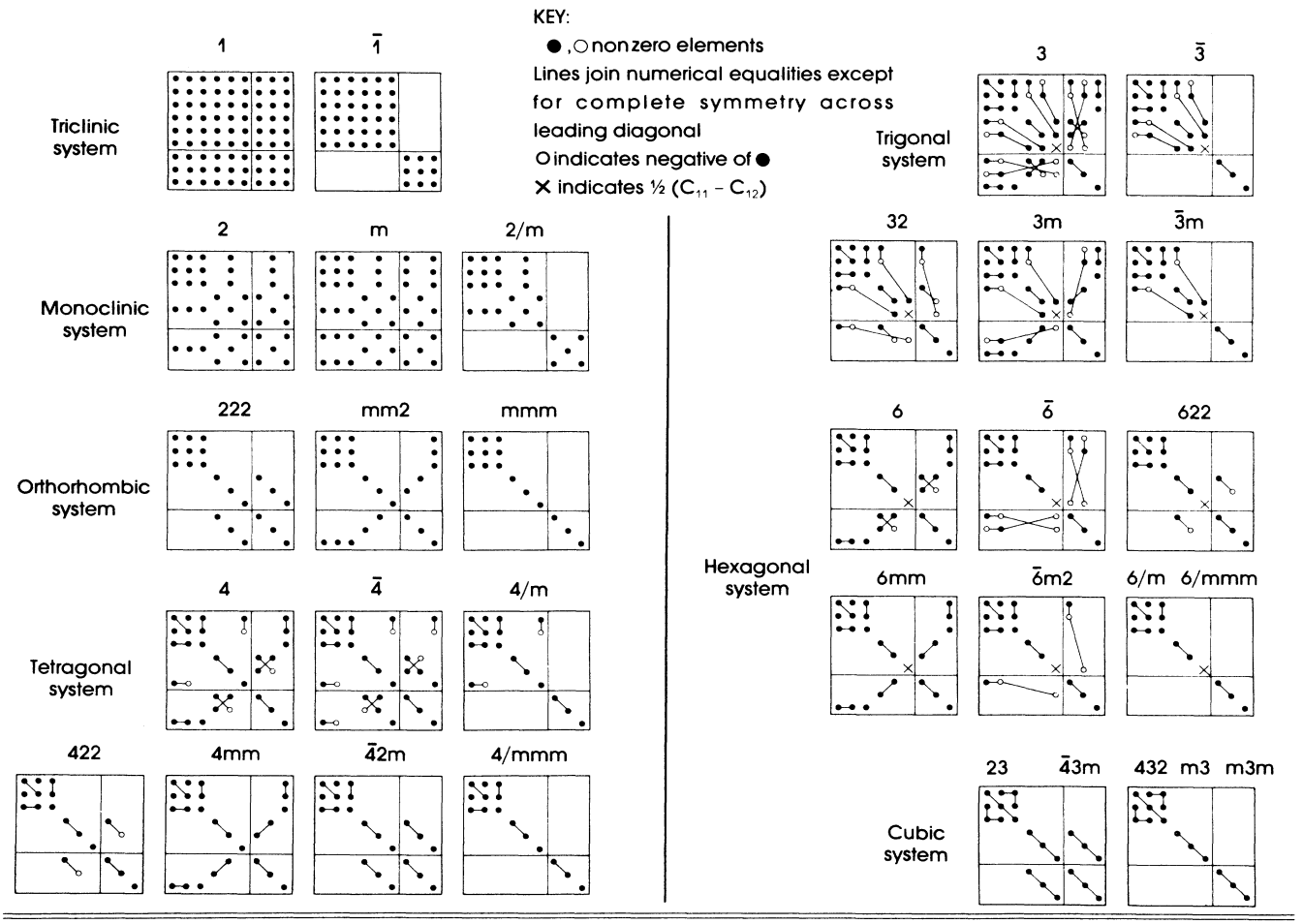

$$\nabla\cdot\mathbf{D}=0 \ . \tag{7}$$

On combining Eqs. (1)–(7) one arrives at the stiffened Christoffel equations

$$(\Gamma_{il}-\rho v^2\delta_{il})U_l=0 \ , \tag{8}$$

where δ_{il} is the δ function and

$$\Gamma_{il}=C_{ijlm}n_j n_m \ , \tag{9}$$

are the Christoffel coefficients. Here $\mathbf{n}=\mathbf{k}/k$ is the wave normal and C_{ijlm} are a set of "piezoelectrically stiffened elastic constants" given by

$$C_{ijlm}=C^E_{ijlm}+\frac{e_{ijr}n_r e_{lms}n_s}{(\epsilon^s_{pq}n_p n_q)} \ . \tag{10}$$

The stiffening of the elastic constants, represented by the second term in Eq. (10), is a function of the permittivity and piezoelectric coefficients, and also depends on the wave normal $\mathbf{n}$. The relative changes to the phase velocities and other attributes of the wave depend on the size of this term in relation to the elastic moduli. Electromechanical coupling constants K defined by expressions of the form

$$K_{ijlm}(\mathbf{n})=\left[\frac{e_{ijr}n_r e_{lms}n_s}{\epsilon^s_{pq}n_p n_q C^E_{ijlm}}\right]^{1/2} , \tag{11}$$

are commonly employed as measures of the strength of the piezoelectric coupling in media, and will be made use of here as well.

Since the stiffening of the elastic constants is quadratic in the piezoelectric coefficients, a simultaneous change in sign of all the e_{ijr} leaves the Christoffel equations unchanged. For cubic and certain other crystal classes where there is only one independent piezoelectric coefficient, it follows that the bulk dynamical properties depend only on the magnitude of this coefficient.

One may go beyond the quasistatic approximation by formally considering the coupling between acoustic and electromagnetic waves in a piezoelectric medium. As shown by Auld,[1] this leads to a slight admixing of acoustic deformation in the electromagnetic waves (which thus become quasielectromagnetic waves) and reciprocal contributions of the electromagnetic field to the acoustic waves (which thus become quasiacoustic waves). However, it is easily shown that this results in corrections to the acoustic velocities which are of the order of a factor v^2/c^2 smaller than the effect of the piezoelectric stiffening. This, for our purposes is too small to be of any consequence, and so this coupled wave mechanism will not be pursued any further.

The first stage in solving the Christoffel equations is to set the secular determinant to zero, i.e.,

$$|\,\Gamma_{il}-\rho v^2\delta_{il}\,|=0 \ . \tag{12}$$

This equation, which is cubic in v^2, has three solutions which are associated with three modes with mutually orthogonal polarizations. One of these modes is usually quasilongitudinal in character and the other two are quasitransverse, although on occasion a different form of identification is more appropriate. These directionally dependent velocities can be represented by a surface of three sheets called the phase velocity surface.

Substituting for Γ_{il} with Eqs. (9) and (10) and multiplying each element of the determinant by $\epsilon=\epsilon^s_{pq}n_p n_q$, Eq. (12) takes on the form

$$|\,E_{iljmrs}n_j n_m n_r n_s-\rho v^2\epsilon_{rs}n_r n_s\delta_{il}\,|=0 \ , \tag{13}$$

where $E_{iljmrs}=C^E_{ijlm}\epsilon_{rs}+e_{ijr}e_{lms}$. If we now multiply each element by v^4, recognizing that $vn_p=(\mathbf{v})_p$, we obtain the equation for the phase velocity surface:

$$|\,E_{iljmrs}v_j v_m v_r v_s-\rho\epsilon_{rs}\delta_{il}v^4 v_r v_s\,|=0 \ , \tag{14}$$

which is of degree 18 in the components of $\mathbf{v}$.

The slowness surface represents the directional dependence of the slowness $\mathbf{S}=(1/v)\mathbf{n}$. It is obtained in a similar way, in this case by dividing each element by v^4:

$$|\,E_{iljmrs}S_j S_m S_r S_s-\rho\epsilon_{rs}\delta_{il}S_r S_s\,|=0 \ . \tag{15}$$

Evidently in its most general form this equation is of degree 12, although it can be less if cancellation of terms occurs. It reduces to degree 6 in the absence of piezoelectric stiffening.[10,11] The higher degree of the slowness surface equation when there is stiffening has important implications for phonon focusing as we will show later.

III. SOLUTION OF THE WAVE EQUATION

A. Solution for special directions

When the wave normal $\mathbf{n}$ lies in a crystallographic mirror plane or in a plane which is perpendicular to a twofold axis of symmetry, one of the three modes is pure transverse, polarized normal to the plane, while the other two modes are mixed modes with polarization vectors lying in the plane. Similarly, when $\mathbf{n}$ points along a twofold axis or normal to a mirror plane, the one mode is pure longitudinal and the other two are transverse. Without any loss of generality we may take the axis or normal to the symmetry plane to lie along the x_2 direction. Since the polarization vector $\mathbf{U}=(0,1,0)$ of the pure mode is an eigenvector of the Christoffel equations, it follows that $\Gamma_{12}=\Gamma_{32}=0$. The corresponding eigenvalue is

$$\rho v_0^2=\Gamma_{22} \ . \tag{16}$$

On factoring out this root from the secular equation, a quadratic equation for the remaining two roots remains, the solutions of which are

$$2\rho v_\pm^2=(\Gamma_{11}+\Gamma_{33})\pm[(\Gamma_{11}-\Gamma_{33})^2+4\Gamma_{13}^2]^{1/2} \ . \tag{17}$$

When $\mathbf{n}$ lies along the special axis in the x_2 direction, the nonvanishing Christoffel coefficients are

$$\begin{aligned}\Gamma_{11}&=C_{66} \ ,\\ \Gamma_{22}&=C_{22} \ ,\\ \Gamma_{33}&=C_{44} \ ,\end{aligned} \tag{18}$$

and

$$\Gamma_{13}=C_{46} \ .$$

For $\mathbf{n}$ lying in the plane, i.e., $\mathbf{n}=(n_1,0,n_3)$, the nonvan-

ishing Christoffel coefficients are

$$\Gamma_{11}=C_{11}n_1^2+C_{55}n_3^2+2C_{15}n_1n_3\ ,$$
$$\Gamma_{22}=C_{66}n_1^2+C_{44}n_3^2+2C_{46}n_1n_3\ , \tag{19}$$
$$\Gamma_{33}=C_{55}n_1^2+C_{33}n_3^2+2C_{35}n_1n_3\ ,$$

and

$$\Gamma_{13}=C_{15}n_1^2+C_{35}n_3^2+(C_{13}+C_{55})n_1n_3\ .$$

If the only crystallographic symmetry is the twofold axis then the point group is monoclinic 2. The nonvanishing elements of the elastic constant, piezoelectric, and permittivity matrices for this and the other crystal classes are indicated in Table I. Using this information and taking **n** along the twofold axis, from Eq. (10) we obtain the stiffened elastic constants $C_{22}=C_{22}^E+e_{22}^2/\epsilon_{22}$, $C_{44}=C_{44}^E$, $C_{66}=C_{66}^E$, and $C_{46}=C_{46}^E$. Hence, from Eqs. (16), (17), and (18) we see that

$$\rho v_0^2=C_{22}^E+e_{22}^2/\epsilon_{22}\ , \tag{20}$$

for the pure L mode, showing that this mode is stiffened by the piezoelectric effect, while the velocities of the two T modes are given by

$$2\rho v_\pm^2=(C_{66}^E+C_{44}^E)\pm[(C_{66}^E-C_{44}^E)^2+4(C_{46}^E)^2]^{1/2}\ , \tag{21}$$

showing that these modes, on the other hand, are not stiffened.

For **n** normal to the twofold axis the stiffened elastic constants are

$$C_{66}=C_{66}^E+(e_{16}n_1+e_{36}n_3)^2/\epsilon\ ,$$
$$C_{44}=C_{44}^E+(e_{14}n_1+e_{34}n_3)^2/\epsilon\ ,$$

and

$$C_{46}=C_{46}^E+(e_{16}n_1+e_{36}n_3)(e_{14}n_1+e_{34}n_3)/\epsilon$$

where

$$\epsilon=\epsilon_{11}n_1^2+\epsilon_{33}n_3^2+2\epsilon_{13}n_1n_3\ ,$$

while the remaining elastic constants remain unstiffened. From Eqs. (16) and (19) we thus obtain

$$\rho v_0^2=C_{66}^En_1^2+C_{44}^En_3^2+2C_{46}^En_1n_3 +[e_{16}n_1^2+(e_{36}+e_{14})n_1n_3+e_{34}n_3^2]^2/\epsilon\ , \tag{22}$$

showing that the pure T mode is stiffened. Since none of the elastic constants entering into the expressions for Γ_{11}, Γ_{33}, and Γ_{13} are stiffened, the velocities for the mixed modes, as given by Eq. (17) are not affected by the piezoelectric coupling.

When the only crystallographic symmetry is a mirror plane the point group is monoclinic m. When **n** is perpendicular to this plane, the pure mode velocity is given by

$$\rho v_0^2=C_{22}^E\ , \tag{23}$$

showing no stiffening, while the velocities of the other two modes, which are stiffened, are given by

$$2\rho v_\pm^2=\left[C_{66}^E+C_{44}^E+\frac{e_{26}^2+e_{24}^2}{\epsilon_{22}}\right] \pm\left[\left[C_{66}^E-C_{44}^E+\frac{e_{26}^2-e_{24}^2}{e_{22}}\right]^2 +4\left[C_{46}^E+\frac{e_{24}e_{26}}{\epsilon_{22}}\right]^2\right]^{1/2}\ . \tag{24}$$

When **n** lies in the mirror plane C_{66}, C_{44}, and C_{46} are unstiffened, while for the remaining elastic constants in Eq. (14),

$$C_{IJ}=C_{IJ}^E+(e_{1I}n_1+e_{3I}n_3)(e_{1J}n_1+e_{3J}n_3)/\epsilon\ .$$

Thus, the velocity of the pure T mode

$$\rho v_0^2=C_{66}^En_1^2+C_{44}^En_3^2+2C_{46}^En_1n_3\ , \tag{25}$$

is unstiffened, while the mixed-mode velocities given by Eq. (17) are stiffened.

To sum up, in general when **n** lies along or is perpendicular to a twofold axis the pure mode undergoes piezoelectric stiffening, while the other two modes are not stiffened. When **n** lies in or is normal to a mirror plane, the converse is true, i.e., the pure mode is unstiffened, while the other two modes are stiffened. If there is additional crystallographic symmetry, the reduced number of independent elastic, piezoelectric, and permittivity coefficients results in a simplification of the expressions for the stiffened elastic constants and velocities. Unstiffened modes remain unstiffened, but it can happen that through the elimination and cancellation of certain terms that a stiffened mode becomes unstiffened. For example, taking $\mathbf{n}\|[100]$ in a tetragonal $4mm$ crystal (e.g., barium titanate), the pure L mode is unstiffened because **n** is perpendicular to the (100) mirror plane ($\rho v^2=C_{11}^E$). The pure T mode polarized in the [010] direction is also unstiffened because **n** lies in the (010) mirror plane ($\rho v^2=C_{66}^E$). It is only the T mode polarized in the [001] direction that is stiffened ($\rho v^2=C_{44}^E+e_{15}^2/\epsilon_{11}$).

Figure 1 depicts a set of principal plane sections of the phase velocity surface of Rochelle salt (orthorhombic 222), illustrating the effect of piezoelectric stiffening on the pure T modes, and absence of stiffening on the mixed modes. (Most of the materials constants used in this and subsequent calculations reported in this paper are listed in Table II.) Actually, the stiffening of the pure T mode for **n** lying in the (100) plane can barely be discerned. This is because the change in ρv^2 for this mode is proportional to $(e_{25}+e_{36})^2$ which happens to be fairly small. The changes in ρv^2 for the pure T modes in the (010) and (001) planes are proportional to $(e_{36}+e_{14})^2$ and $(e_{25}+e_{14})^2$, respectively. Both of these factors contain the coefficient e_{14}, which for Rochelle salt is extremely large, hence, the very large stiffening of the T modes for these two planes. A twofold axis, which in addition is normal to a mirror plane, implies the existence of a center of inversion, and thus there can be no piezoelectric effect.

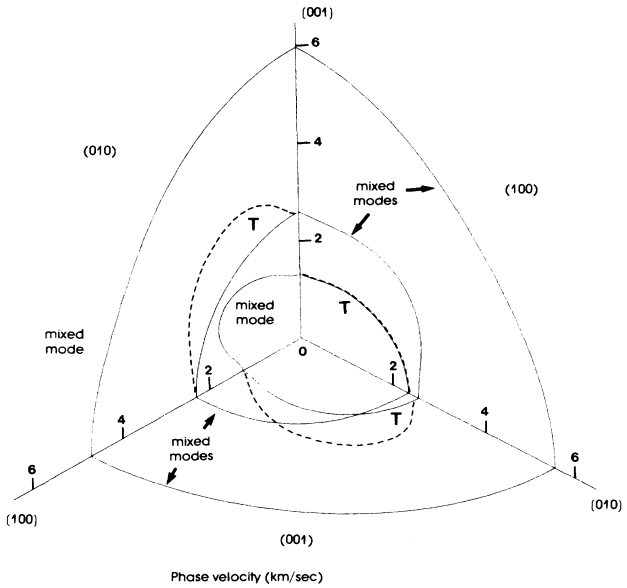

FIG. 1. Principal plane sections of the phase velocity surface of Rochelle salt: —— the unstiffened modes, — — — the stiffened pure T mode.

B. General solution

In general, when $\mathbf{n}$ does not lie along a symmetry axis or in a symmetry plane, all three modes are of mixed character and the secular determinant for the Christoffel equations does not factorize. In this situation it is convenient to solve the cubic equation for v^2 by the method of trigonometric functions.[14] In phonon imaging calculations quantities such as phase and group velocities and polarization vectors, etc., have to be computed for a very large number of wave normals. One therefore seeks to structure the solution in a form which makes for easy translation into efficient computer code. The method outlined below, we have found, is reasonably satisfactory in this regard.

Making the replacement

$$\epsilon\rho v^2=\frac{\lambda+T}{3} \tag{26}$$

in Eq. (13), where

$$T=F_{jmrs}n_jn_mn_rn_s\ , \tag{27}$$

and $F_{jmrs}=E_{iijmrs}$, one arrives at the equation

$$|\Lambda_{il}-\lambda\delta_{il}|=0\ , \tag{28}$$

where

$$\Lambda_{il}=B_{iljmrs}n_jn_mn_rn_s\ , \tag{29}$$

is a traceless tensor and $B_{iljmrs}=3E_{iljmrs}-\delta_{il}F_{jmrs}$. On expanding the determinant in Eq. (28) one obtains the equation for λ in the form

$$\lambda^3-3G\lambda-2H=0\ , \tag{30}$$

where

$$G=\tfrac{1}{6}\Lambda_{il}\Lambda_{il}\ , \tag{31}$$

$$H=\tfrac{1}{2}\epsilon_{rst}\Lambda_{1r}\Lambda_{2s}\Lambda_{3t}\ , \tag{32}$$

and ϵ_{rst} is the alternating symbol. The three solutions to Eq. (30) can be written in the form

$$\lambda_n=2G^{1/2}\cos(\psi+\tfrac{2}{3}\pi n),\quad n=0,1,2\ , \tag{33}$$

where

$$\psi=\tfrac{1}{3}\arccos(H/G^{3/2})\ . \tag{34}$$

In the computation of a phonon image the constant tensors F and B need to be calculated only once, at the outset. These are then contracted with each value of $\mathbf{n}$ with respect to four indices to obtain T and Λ_{il}; G and H are then calculated, and v is obtained from Eqs. (26), (33), and (34).

C. Calculation of group velocity

The group velocity $\mathbf{V}=\partial\omega/\partial\mathbf{k}$ is required for the evaluation of phonon flux. In the absence of dispersion $\mathbf{V}$ is given by

$$\mathbf{V}=\left[v-\mathbf{n}\frac{\partial v}{\partial\mathbf{n}}\right]\mathbf{n}+\frac{\partial v}{\partial\mathbf{n}}\ . \tag{35}$$

It is evident from Eq. (13) that v is a homogeneous function of degree 1 in the components of $\mathbf{n}$. It follows from Euler's theorem therefore that the term in parentheses vanishes, and hence that

$$\mathbf{V}=\frac{\partial v}{\partial\mathbf{n}}\ . \tag{36}$$

One way of evaluating $\mathbf{V}$ is by implicit differentiation on the Christoffel linear equations. Differentiating Eq. (8) with respect to n_α, multiplying the result by U_i and using the normalization condition $U_iU_i=1$ one arrives at the expression

$$V_\alpha=\frac{1}{2\rho v}\frac{\partial\Gamma_{il}}{\partial n_\alpha}U_iU_l\ . \tag{37}$$

From the defining Eqs. (9) and (10) for Christoffel tensor Γ_{il} it follows that

$$V_\alpha=\left[2C^E_{i\alpha lm}n_m+\frac{\partial}{\partial n_\alpha}\left[\frac{e_{ijr}n_jn_re_{lms}n_mn_s}{\epsilon^s_{pq}n_pn_q}\right]\right]\frac{U_iU_l}{2\rho v}\ . \tag{38}$$

Another method, which obviates the need to calculate the polarization vectors for the modes, is to obtain $\partial v/\partial\mathbf{n}$ by implicit differentiation on the Christoffel secular equation. Proceeding in this manner, making use of Eqs. (26) and (30), one obtains

$$V_\alpha=\frac{1}{6\rho v\epsilon}\left[\frac{\partial T}{\partial n_\alpha}+\frac{\partial\lambda}{\partial n_\alpha}\right]-\frac{v}{\epsilon}\epsilon_{\alpha\beta}n_\beta\ , \tag{39}$$

where

TABLE II. Values taken for the elastic constants, relative permittivities, piezoelectric stress coefficients, and densities of the crystals treated in this paper. They have been taken from Refs. 1, 9, 12, and 13. In some cases where several values of the same quantity were available, an average or interpolated value has been adopted.

	$Bi_{12}GeO_{20}$	CuCl	$LiIO_3$	$AlPO_4$	$LiTaO_3$	$BaTiO_3$	$LiGaO_2$	$Ba_2NaNb_5O_{15}$	Rochelle salt
C (GPa)									
C_{11}	125.0	45.4	81.2	64.0	230	275	140	239	39.8
C_{22}							120	247	55.3
C_{33}			52.9	85.8	276	165	140	135	63.2
C_{44}	25.3	13.6	17.8	43.2	95.9	54.4	57.1	65	11.9
C_{55}							47.4	66	3.05
C_{66}						113	69.0	76	9.95
C_{12}	33.0	36.3	31.8	7.2	42	179	14	104	24.3
C_{13}			9.2	9.6	79	152	28	50	31.9
C_{14}				−12.4	−11				
C_{23}							31	52	23.8
ϵ_{11}	38	8	7.9	6	43	1970	7.0	222	115
ϵ_{22}							6.5	227	8.4
ϵ_{33}			5.9	6	43	109	8.3	32	9.4
e (C/m^2)									
e_{11}				−0.54					
e_{14}	1.0	0.41	0.10	−0.16					4.00
e_{15}			0.89		2.7	21.3	−0.32	2.8	
e_{22}					2.0				
e_{24}							−0.34	3.4	
e_{25}									−0.15
e_{31}			0.65		−0.1	−2.74	−0.17	−0.4	
e_{32}							−0.31	−0.3	
e_{33}			0.97		2.0	3.70	0.96	4.3	
e_{36}									0.11
Density (kg/m^2)	9200	4140	5402	2566	7450	6017	4187	5300	1767
Crystal class	23	$\bar{4}3m$	6	32	$3m$	$4mm$	$mm2$	$mm2$	222
References	9,12	9,12	9,12	12,13	9,12	1,9,12	9,12	9,12	9,12

$$\frac{\partial\lambda}{\partial n_\alpha}=\left[\lambda\frac{\partial G}{\partial n_\alpha}+\frac{2}{3}\frac{\partial H}{\partial n_\alpha}\right]\Big/(S^2-G)\ . \tag{40}$$

The derivatives $\partial T/\partial n_\alpha$, $\partial G/\partial n_\alpha$, and $\partial H/\partial n_\alpha$ are obtained in a straightforward manner from the defining Eqs. (27), (29), (31), and (32) for T, G, and H. For instance,

$$\frac{\partial T}{\partial n_\alpha}=F^{(1)}_{\alpha lrs}n_l n_r n_s\ , \tag{41}$$

where

$$F^{(1)}_{\alpha lrs}=F_{\alpha lrs}+F_{l\alpha rs}+F_{lr\alpha s}+F_{lrs\alpha} \tag{42}$$

is a constant tensor for a material.

IV. PHONON FOCUSING

A. Monte Carlo phonon image calculations

A phonon image portrays the directional dependence of the phonon flux emanating from a localized heat source in a crystal.[3] We will follow a common procedure used in the Monte Carlo calculation of phonon images which is to assume a uniform distribution of wave normal directions, calculate the ray vectors **V** for each of these normals, and then sort these **V**'s in direction to form a polar plot of the phonon intensity, summing over phonon branches as desired.[16] This procedure ignores the role of surface directivity effects,[17] and takes no account of directional and branch dependence of the mode heat capacity. It does, however, have the advantage of simplicity, and it emphasizes the role of phonon focusing which is the major source of anisotropy in the phonon flux.

A number of intensity plots calculated in this way are provided in later sections of this paper. Each of these is composed of approximately 3×10^5 ray vectors. The acoustic symmetries[18] of the crystals considered have been used to map each ray vector into its symmetry equivalent positions thereby considerably reducing computational time. The calculations have been done on an IBM 3083 mainframe computer and take approximately 1 min of CPU time per image where there is a high degree of sym-

metry to be exploited, and proportionality more where there is less symmetry.

B. Phonon focusing and the slowness surface

The phonon flux emanating from a point heat source in a crystal is, in general, highly anisotropic, and caustics along which the flux is mathematically infinite are a common occurrence.[16,19] This phenomenon has a simple interpretation in terms of the shape of the phonon constant frequency or slowness surface.[20] Phonon ray vectors $\mathbf{V}=\partial\omega/\partial\mathbf{n}$ are required to be perpendicular to this surface, and so the extent to which these rays are bunched or focused in any particular direction is inversely proportional to the Gaussian curvature K of the surface. The phonon focusing or enhancement factor A describing this effect is given by[16,21,22]

$$A^{-1}=|S^3VK| \ . \tag{43}$$

The slowness surface for a typical crystal will possess negatively and positively curved regions. The zero curvature or parabolic lines separating these regions map on to focusing caustics. The topology of the slowness surface is of considerable interest in understanding phonon-focusing patterns. The curvature of this surface is given by

$$K=\frac{v^4}{V^4}(\beta_{22}\beta_{33}+\beta_{33}\beta_{11}+\beta_{11}\beta_{22}-\beta_{12}^2-\beta_{23}^2-\beta_{31}^2) \ , \tag{44}$$

where

$$\beta_{ij}=\frac{\partial^2 v}{\partial n_i \partial n_j} \ . \tag{45}$$

These second-order derivatives are obtainable in a straightforward way by implicit differentiation on Eqs. (26) and (30) and expressions similar to, but somewhat more complicated than, those in Eqs. (39) and (40) emerge. We have used these results to locate the regions of different curvature on the slowness surface depicted later in Fig. 11(d).

A fundamental constraint on phonon focusing in nonpiezoelectric crystals in the long-wavelength continuum limit is that the fast phonon branch (which is usually, but not always, associated with longitudinally polarized modes) cannot form focusing caustics. In order to do so, the inner sheet of the slowness surface would have to possess negatively curved regions, and hence it would be possible to find a straight line passing eight or more times through the complete three-sheeted surface.[23] Since the equation of the slowness surface is of degree 6, this is not possible.

This constraint does not apply to piezoelectric crystals for, as we have seen, the equation for the slowness surface for such crystals is, in general, of degree 12. Later in this paper we provide two examples of crystals which do indeed have fast phonon branch caustics.

V. PHONON FOCUSING IN CUBIC CRYSTALS

Phonon focusing in nonpiezoelectric cubic crystals has been the subject of a number of investigations.[22,24–26] The focusing patterns of these crystals depend on two parameters, the elastic constant ratios $a=C_{11}/C_{44}$ and $b=C_{12}/C_{44}$. Two of the five cubic crystal classes, $\bar{4}3m$ and 23, are permitted a piezoelectric effect. In both cases, as shown in Table I, the piezoelectric matrix has the same form, comprising only one independent coefficient e_{14}. It is therefore sufficient to define a single electromechanical coupling constant $K_{44}=(e_{14}^2/\epsilon_{11}^s C_{44}^E)^{1/2}$. Rather than attempt here a complete classification of all the focusing patterns that can exist subject to the three control parameters a, b, and K_{44}, we will limit the discussion to some actual materials and their neighboring regions of parameter space.

Figure 2 shows the location on an (a,b) plot of the more strongly piezoelectric crystals that are known based on data from the tabulations of Cook and Jaffe,[9] Hearmon,[12] and Cook.[13] The crystals essentially fall into three main categories. A few are nearly elastically isotropic, i.e., have $a\approx b+2$; there are some of fairly large and positive elastic anisotropy $\Delta=a-b-2$, and a number of fairly large and negative elastic anisotropy Δ.

The influence of piezoelectric stiffening is greatest when a crystal is elastically isotropic or nearly so. We will discuss this category of crystals in some detail because they display phenomena which differ markedly from those of nonpiezoelectric media. Crystals falling into this category are $Bi_4Ge_3O_{12}$, $Bi_4Si_3O_{12}$ and $K_2Mg_2(SO_4)_3$.

In the limit $\Delta=0$ and $K_{44}=0$ the ST and FT phonon branches are completely degenerate and all three sheets of

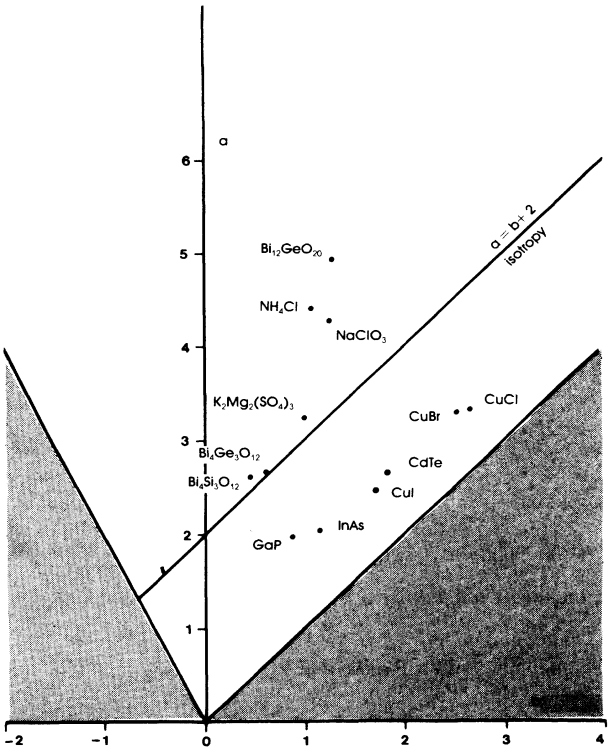

FIG. 2. Elastic constant ratios of the more strongly piezoelectric cubic crystals ($a=C_{11}/C_{44}$ and $b=C_{12}/C_{44}$).

the slowness surface are spherical. There is no focusing whatsoever. With $\Delta=0$ and K_{44} allowed to deviate from zero the ST sheet remains spherical, with radius $(\rho/C_{44}^{E})^{1/2}$ while the FT sheet contracts inwards everywhere except in the $\langle 100\rangle$ and $\langle 111\rangle$ directions where it maintains tangential contact with the ST sheet. There are *not* the familiar conical degeneracies in the $\langle 111\rangle$ directions that exist when $K_{44}=0$ and $\Delta\neq 0$. The polarization field for the two modes possesses singularities at the degenerate points.[27] In a small circuit around one of these degenerate points the polarization field rotates by $2\pi n$, where the rotary index $n=+1$ or -1. Near the $\langle 111\rangle$ degenerate points the FT polarization field points radially outwards while the ST polarization is circumferential. The rotary index of this degeneracy is therefore $n=+1$. For the $\langle 100\rangle$ degeneracies the polarization field has rotary index $n=-1$. For moderate values of K_{44} (providing Δ remains zero) all three sheets of the slowness surface are entirely convex and there are no focusing caustics.

If K_{44} is now fixed at some value and Δ allowed to deviate from zero, each $\langle 111\rangle$ tangential degeneracy is transformed into an $n=-\frac{1}{2}$ point of conical degeneracy in the $\langle 111\rangle$ direction and three $n=+\frac{1}{2}$ conical points symmetrically positioned around that $\langle 111\rangle$ direction in the $\{110\}$ planes. For $\Delta>0$ and increasing, the three $n=+\frac{1}{2}$ conical points move towards the neighboring $\langle 110\rangle$ directions. Figure 3 depicts the ST sheet of the slowness surface and the associated polarization field at this stage. The elastic, piezoelectric, and permittivity constants for the calculation are those of $Bi_4Ge_3O_{12}$, except that the value of C_{11} has been reduced from 116.0 to 114.21 GPa. The conical points are labeled C and are clearly the location of singularities in the polarization field. As Δ increases further, pairs of conical points approaching from opposite sides meet in the $\langle 110\rangle$ directions, break apart again, and then move along the $\{100\}$ planes until finally merging with the $\langle 100\rangle$ degeneracies, labeled D, to form $n=+1$ tangential degeneracies. It is interesting to note that the value of the electromechanical coupling constant used in the calculations for Fig. 3, $K_{44}=0.015$, is very small and yet has a profound effect on the topology of the slowness surface, establishing acoustic axes (the additional conical points) where none occur for nonpiezoelectric cubic crystals. The reason for this is that the piezoelectric stiffening is in direct competition with the residual elastic anisotropy in lifting the degeneracy of the transverse sheets of the slowness surface. Well before C_{11} reaches the value 116.0 GPa of $Bi_4Ge_3O_{12}$ the elastic anisotropy becomes dominant, and the effect of the electromechanical coupling is "quenched." For $\Delta<0$ and increasing in magnitude, the three $n=+\frac{1}{2}$ conical points move towards their nearest $\langle 100\rangle$ directions where they merge with the $n=-1$ degeneracies there to form $n=+1$ tangential degeneracies.

The emergence of the conical points for either $\Delta>0$ or $\Delta<0$ is accompanied by the formation of ST branch caustics. For small Δ and K_{44} these caustics are very faint, however, on account of the deviation of the slowness surface from spherical being so slight. A polar plot of the ST phonon intensity of a hypothetical sample where both $|\Delta|$ and K_{44} are of moderate size is shown in Fig. 4. The pairs of prominent cusps, located approximately midway between the $\langle 100\rangle$ and neighboring $\langle 111\rangle$ directions, are positioned alongside conical points.

The second category comprises crystals such as $Bi_{12}GeO_{20}$, NH_4Cl, and $NaClO_3$ which have large and

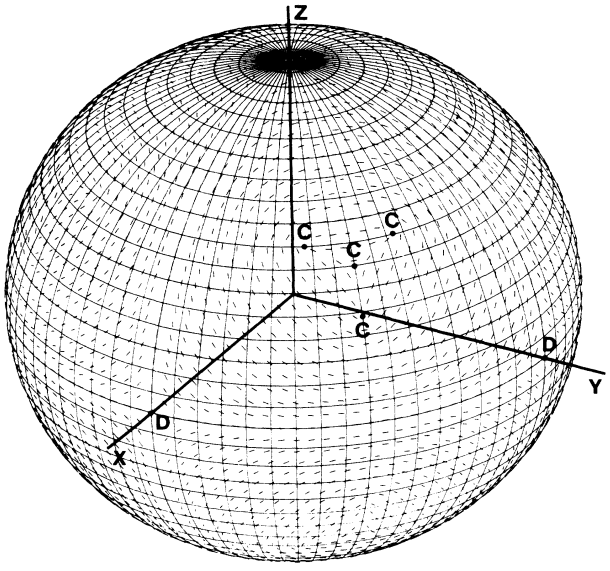

FIG. 3. The ST sheet of the slowness surface of a medium with $C_{11}=114.21$ GPa, $C_{12}=27.0$ GPa, $C_{44}=43.6$ GPa, $e_{14}=0.038$ C/m^2, and relative permittivity $\epsilon_{11}=16$. Conical points are labeled C, and tangential degeneracies are labeled D.

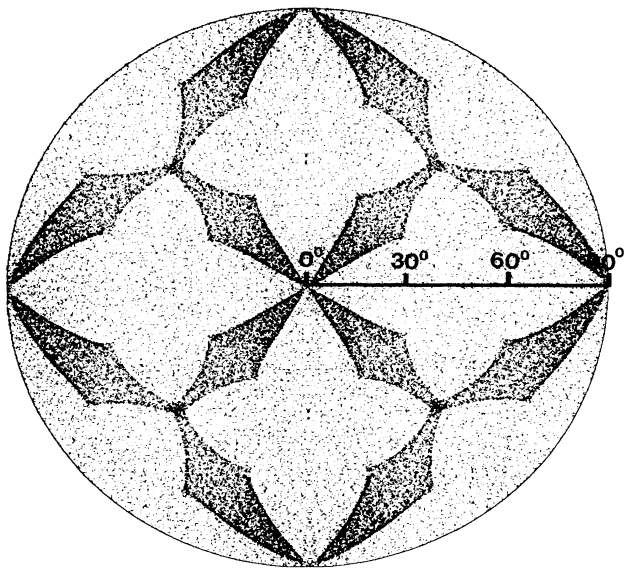

FIG. 4. Polar plot of the ST phonon intensity for a medium with $C_{11}/C_{44}=2.39$, $C_{12}/C_{44}=0.62$, and $K_{44}=0.4$. Phonon intensity corresponds to the darkness of the plot.

positive elastic anisotropy. We have not found any crystals in this category for which the piezoelectric stiffening is large enough to change the topology of the slowness surface and the focusing pattern. The changes that do occur are merely qualitative alterations in the positions and shapes of the focusing caustics. As an example, $Bi_{12}GeO_{20}$ (class 23) is a crystal with a particularly large piezoelectric effect, having $K_{44}=0.34$. Figure 5(a) shows the calculated ST and FT focusing pattern of this crystal when piezoelectric stiffening is neglected. This type of focusing pattern is displayed by numerous crystals such as CaF_2 and CsCl, etc., and has been discussed in detail by Every[22] and Hurley and Wolfe.[26] Figure 5(b) shows the flux pattern of $Bi_{12}GeO_{20}$ when piezoelectric stiffening is included. The most significant changes are to the shapes of the ST caustics. These form much narrower structures than before, and are more rounded, particularly near to the ⟨111⟩ directions.

A large proportion of piezoelectric cubic crystals fall into the third category, having negative anisotropy Δ. Examples are III-V and II-VI compounds such as GaP, InAs, and CdTe and the copper halides CuCl, CuBr, and CuI. The latter group of crystals are interesting for their anomalous dynamical properties,[28] and all have particularly large electromechanical coupling. Figure 6(a) shows the calculated FT and ST phonon intensity pattern for

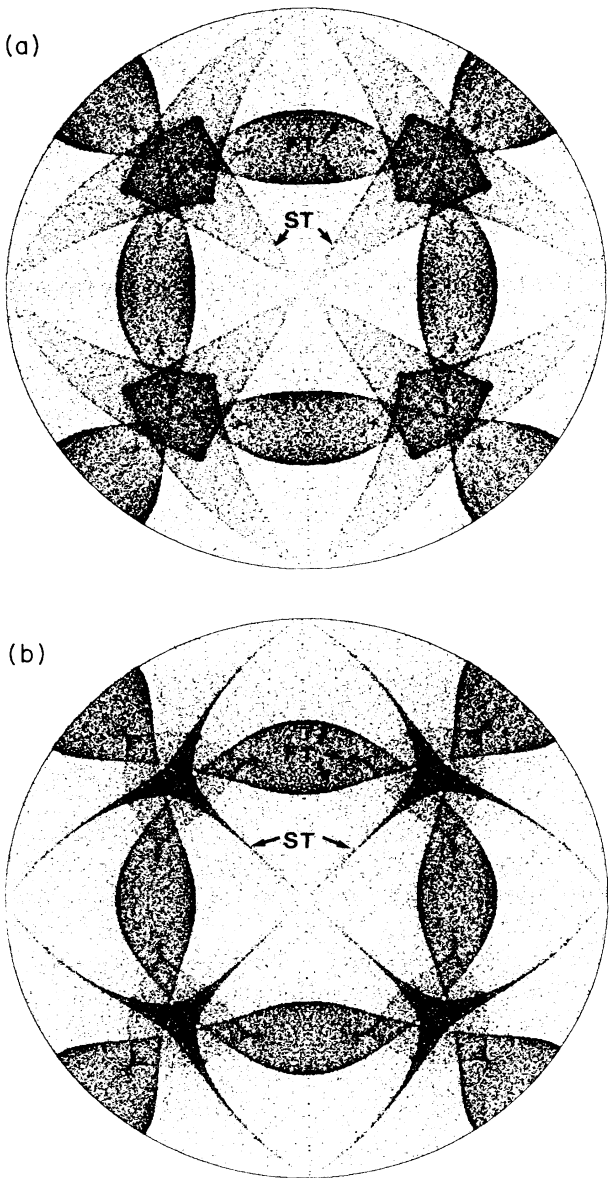

FIG. 5. Polar plot of the ST and FT phonon intensity pattern of $Bi_{12}GeO_{20}$ (a) with the piezoelectric effect ignored, (b) with piezoelectric stiffening included.

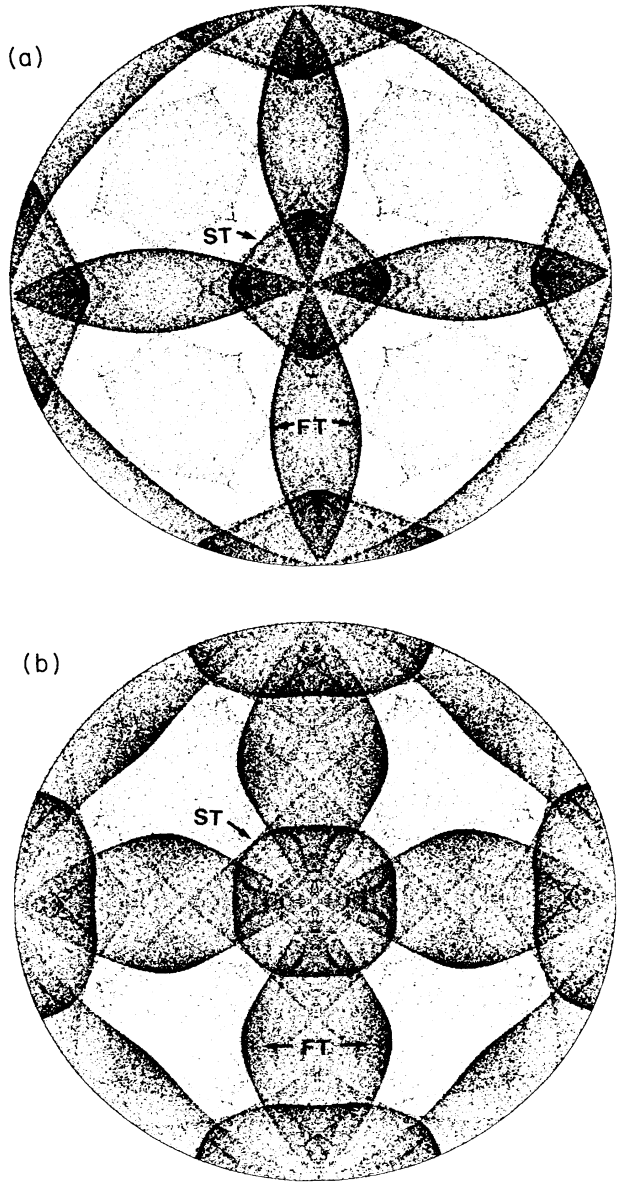

FIG. 6. Polar plot of the ST and FT phonon intensity pattern of CuCl (a) with the piezoelectric effect ignored, (b) with piezoelectric stiffening included.

CuCl (class $\bar{4}3m$) with the piezoelectric effect ignored. It is the well-known pattern displayed by Ge, Si, and numerous other cubic crystals.[16,22,26] Figure 6(b) shows the modified intensity pattern when the piezoelectric effect is taken account of. In spite of the very large electromechanical coupling constant ($K_{44}=0.42$) there are no new topological features, merely qualitative changes to the existing caustics. The pairs of FT caustics running between neighboring $\langle 100 \rangle$ directions are further apart and somewhat distorted in shape. The ST boxlike structure around the [001] direction has a more rounded appearance, and the "Maltese-cross" structure inside the box is more highly developed.

VI. PHONON FOCUSING IN OTHER CRYSTAL SYSTEMS

For crystals having several independent piezoelectric coefficients there are numerous different electromechanical coupling constants that can be defined, none of which solely provide a complete characterization of the influence of the piezoelectric stiffening. It is desirable, however, to choose a single suitable parameter by which the strength of the piezoelectric coupling can roughly be gauged. Since most of the materials we will be discussing in this section are drawn from crystal classes for which $e_{14}=0$ so that $K_{44}=0$, we will be making reference instead to the values of $K_{33}=(e_{33}^2/\epsilon_{33}^s C_{33}^E)^{1/2}$ or $K_{11}=(e_{11}^2/\epsilon_{11}^s C_{11}^E)^{1/2}$, whichever happens to be nonzero. In the case of Rochelle salt (class 222) we will quote K_{44} since $K_{11}=K_{33}=0$.

A. Hexagonal system

As can be seen in Table I, the elastic constant matrix has the same form for all seven of the hexagonal crystal classes. This form of the elastic constant matrix is in fact invariant under all rotations about the Z axis, and consequently, in the absence of the piezoelectric effect, hexagonal crystals possess transverse acoustic isotropy. The phonon-focusing patterns that nonpiezoelectric hexagonal crystals display have been described by McCurdy[29] and Every.[30]

Five of the hexagonal classes lack a center of inversion and are permitted a piezoelectric effect. Classes 6, $6mm$, and 622 have piezoelectric and permittivity tensors which are invariant under rotations about the Z axis. These classes therefore retain their transverse-acoustic isotropy under piezoelectric stiffening of the elastic constants. Figure 7(a) depicts a meridian section of the slowness surface of $LiIO_3$ (class 6) both with and without piezoelectric stiffening. Because of the very large electromechanical coupling ($K_{33}=0.58$), there is a substantial difference between the two cases. With stiffening the quasi-T slowness curve is pulled inwards to such an extent that it no longer intersects the pure-T curve, and the angular widths of the negatively curved regions of this curve are reduced from 22° to 5°. Figure 7(b) shows the corresponding section through the group velocity surface. The effect of stiffening on the quasi-T velocity curve is to cause it to bulge outwards near the [100] direction and to bring the pairs of cusps so close together that they can not easily be resolved.

As shown by Every,[18] the piezoelectric matrices for classes $\bar{6}$ and $\bar{6}m2$ are not rotationally invariant about the Z axis, and so these classes lose their transverse isotropy under stiffening of the elastic constants. The acoustic symmetry for both these classes reverts to $6/mmm$. The effects are most dramatic for crystals like GaSe for which the two transverse sheets intersect in the absence of the piezoelectric effect. Stiffening of the elastic constants causes these lines of wedge-shaped degeneracy to be replaced by a small number of points of conical degeneracy, and an associated pattern of caustics emerges.

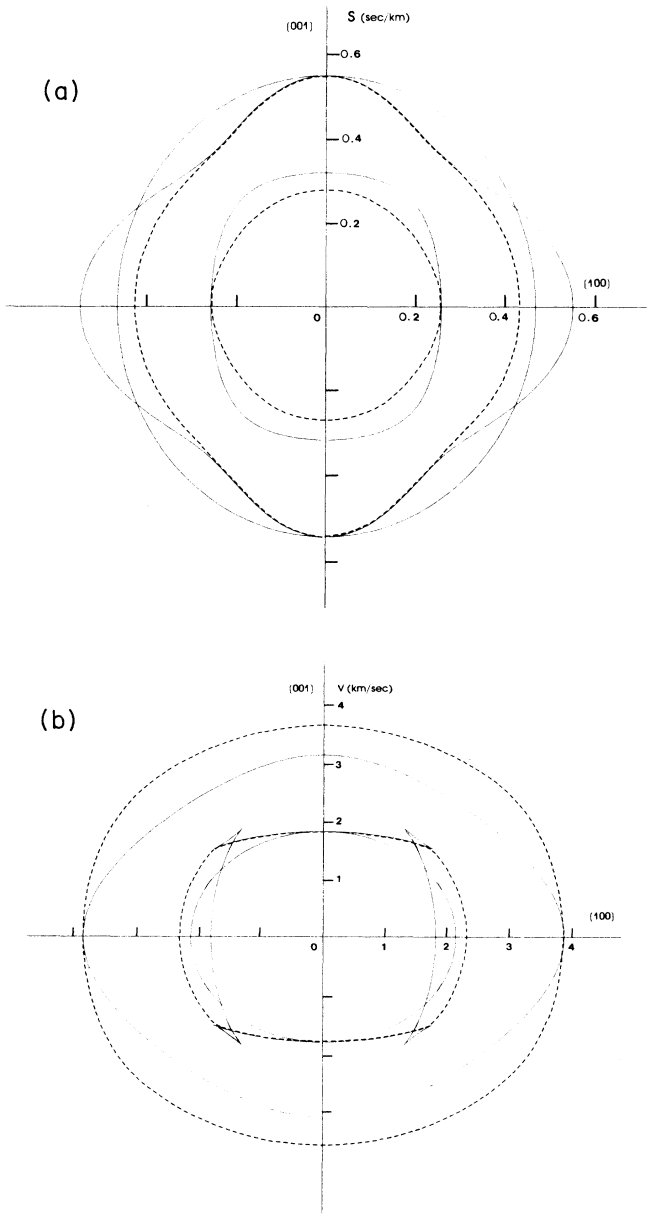

FIG. 7. (a) Meridian section of the slowness surface of $LiIO_3$ —— without piezoelectric stiffening, — — — with piezoelectric stiffening. (b) Corresponding group velocity curves.

B. Trigonal system

Two of the technologically most important piezoelectric crystals, quartz and $LiNbO_3$, belong to the trigonal system. Phonon imagining has been carried out on both these materials by Koos and Wolfe.[7] In the case of $LiNbO_3$ the effects of piezoelectric stiffening of the elastic constants are quite dramatic. The FT phonon branch acquires a prominent set of caustics that meander above and below the (001) plane, while the ST caustics become fragmented and reduced in extent. Quartz, on the other hand, has appreciably smaller electromechanical coupling constants, and piezoelectric stiffening has a barely perceptible effect on the focusing pattern.[7,31] Three other trigonal crystals which are exceptional as regards the large size of their electromechanical coupling constants are $AlPO_4$, tellurium (Te), and $LiTaO_3$.

The ST and FT phonon intensity pattern for $AlPO_4$ (class 32) in the absence of the piezoelectric effect is shown in Fig. 8(a). It is almost indistinguishable from that of quartz. However, the electromechanical coupling constant for $AlPO_4$ ($K_{11}=0.293$) is much larger than that of quartz ($K_{11}=0.093$), and the focusing pattern, as shown in Fig. 8(b), is considerably changed by stiffening. The caustics labeled *A* bulge out much further than before and the ridge of large but finite phonon intensity (precursor) labeled *B* has evolved into a pair of caustics.

The phonon intensity pattern of tellurium (class 32)

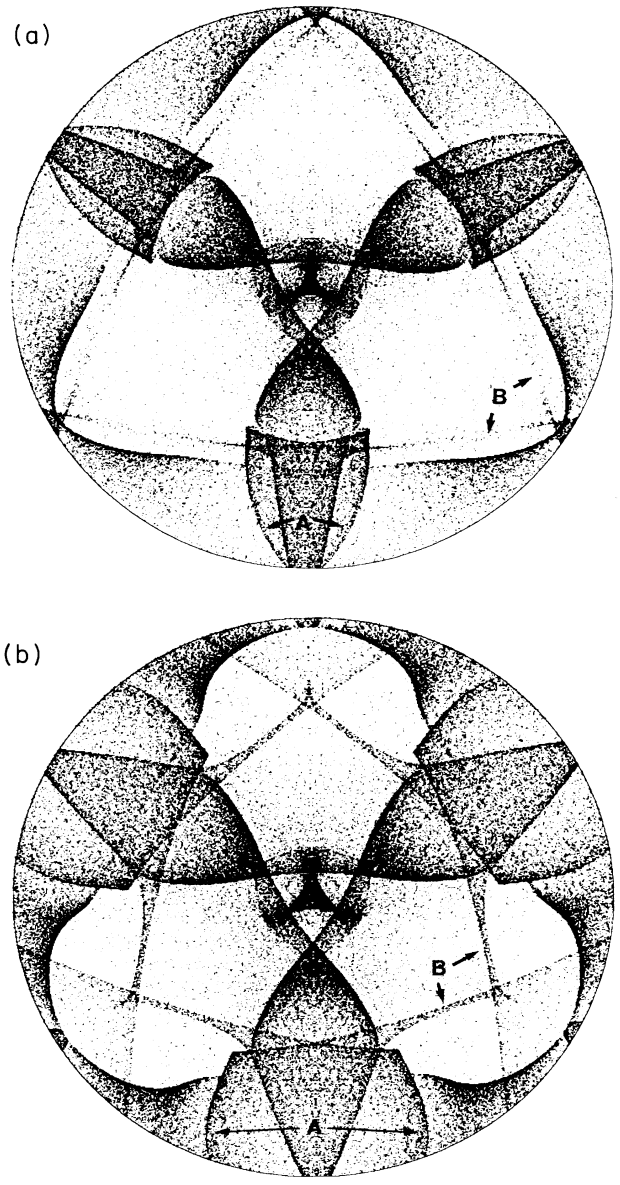

FIG. 8. Polar plot of the ST and FT phonon intensity of $AlPO_4$ (a) without piezoelectric effect, (b) with piezoelectric effect.

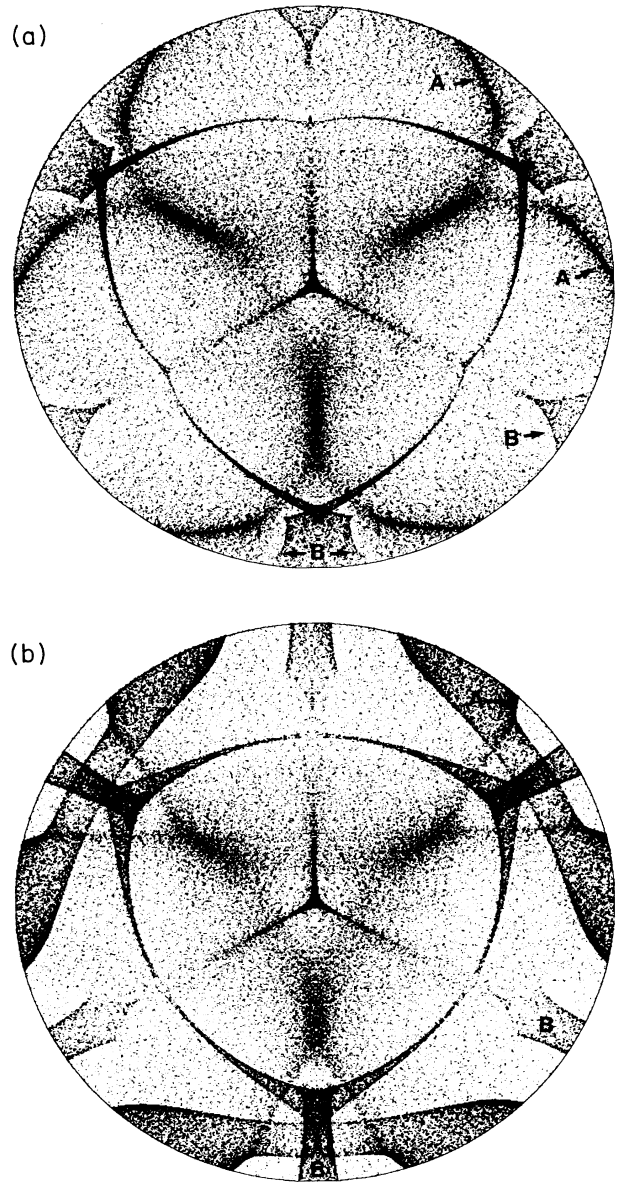

FIG. 9. Polar plot of the ST and FT phonon intensity of $LiTaO_3$ (a) without piezoelectric effect, (b) with piezoelectric effect.

also bears some resemblance to that of quartz. The effect of the piezoelectric stiffening for Te ($K_{11}=0.34$) is even greater than for $AlPO_4$. The bulging out of feature A is more pronounced, and there is a considerable modification to the focusing structures in the vicinity of the Z axis.

The phonon intensity pattern of $LiTaO_3$ (class $3m$) before and after the inclusion of the piezoelectric effect is shown in Figs. 9(a) and 9(b) ($K_{33}=0.195$). The most noticeable result of the stiffening is the transformation of the FT structure A into a pair of caustics that meander above and below the (001) plane. The intense band thus formed is almost identical in appearance to the corresponding feature in $LiNbO_3$. The ST focusing structure labeled B has no counterpart in $LiNbO_3$. The effect of the stiffening is to cause it to become narrower and more elongated.

C. Tetragonal system

Phonon focusing in nonpiezoelectric tetragonal crystals has been surveyed by Winternheimer and McCurdy.[32] Five of the tetragonal classes, namely 4, $\bar{4}$, 422, $4mm$, and $\bar{4}2m$, lack a center of inversion and are permitted a

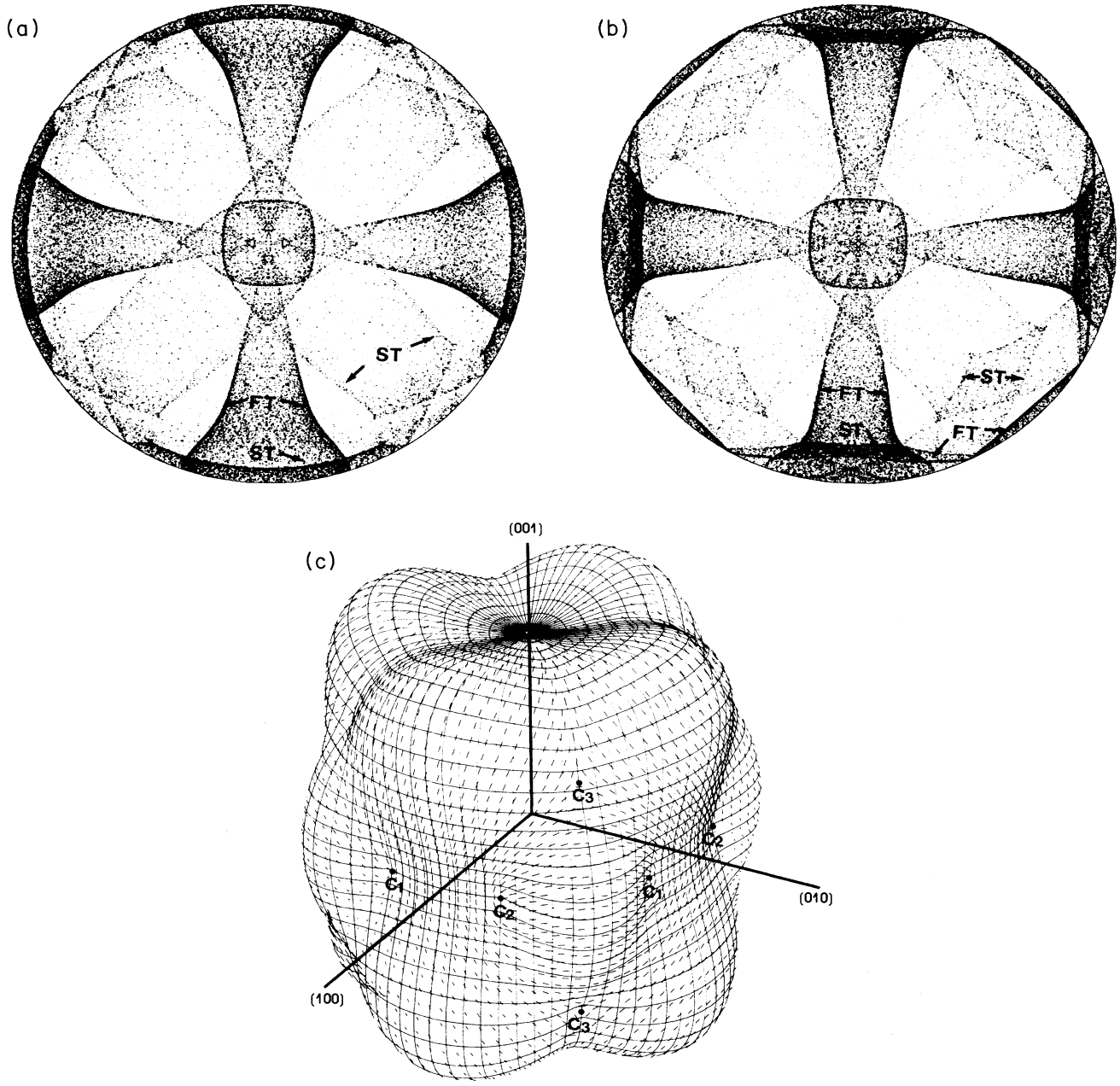

FIG. 10. Polar plot of the ST and FT phonon intensity of $BaTiO_3$ (a) without piezoelectric effect, (b) with piezoelectric effect. (c) ST sheet of the slowness surface of $BaTiO_3$.

piezoelectric effect. To date, the only tetragonal crystal on which experimental phonon imaging has been reported is TeO_2 (class 422).[33] This material is unusual in its exceptionally high degree of elastic anisotropy. As a result the phonon images which Hurley, Wolfe, and McCarthy[33] have obtained depend very much on where the time gates are set for acceptance of the arriving phonon flux. As noted by these authors the electromechanical coupling is small, changing the elastic constants by less than 1% and having little influence on the phonon focusing.

Of the crystals on which data is available, the one whose phonon focusing is most strongly influenced by piezoelectric stiffening is $BaTiO_3$ (class $4mm$). Figure 10(a) shows the ST and FT phonon intensity pattern when the piezoelectric effect is ignored, and Fig. 10(b) shows the modified pattern when stiffening of the elastic constants is included ($K_{33}=0.29$). The largest changes come about in a region extending approximately 30° on either side of the (001) plane, and affect both the ST and FT branches. This phonon intensity pattern bears a remarkable resemblance to the focusing patterns of the negative anisotropic cubic crystals such as CuCl discussed earlier, particularly in the region of the Z axis. The similarity is brought home even more by an inspection of the slowness surface of $BaTiO_3$. Fig. 10(c) shows the ST sheet of this surface. The topology of this surface and the associated polarization field are almost identical to that of crystals like GaAs and CuCl, except that in place of $n=+1$ tangential degeneracies in the [100] and [010] directions there are pairs of $n=+\frac{1}{2}$ conical points labeled C_1 and C_2 to either side of these directions in the (001) plane.

There are a number of crystals related to $BaTiO_3$ which have even larger electromechanical coupling coefficients. Complete sets of piezoelectric stress coefficients are, however, not available for most of these. We note in passing that the material $Sr_4KLiNb_{10}O_{30}$ (class $4mm$) has very large electromechanical coupling ($K_{33}=0.54$) but exhibits little phonon focusing and no caustics either with or without piezoelectric stiffening. This is partly attributable to the fact that the elastic constants satisfy the condition for transverse isotropy, $C_{66}=\frac{1}{2}(C_{11}-C_{12})$, and so do the piezoelectric and permittivity coefficients.

D. Orthorhombic system

Several of the most strongly piezoelectric crystals belong to the orthorhombic crystal classes 222 and $mm2$. The best known of these is Rochelle salt (class 222). Figures 11(a) and 11(b) show the ST and FT phonon intensity patterns before and after the inclusion of piezoelectric stiffening ($K_{44}=1.15$). While there are some features which are recognizably shared by both patterns, stiffening of the elastic constants has the effect of eliminating the very prominent crescent-shaped structures A, which are slightly unfolded lips events,[34] and rendering the overall pattern of caustics much more complex. Even more remarkable is the effect that electromechanical coupling has on the longitudinal phonon branch. The intensity pattern for this branch coupling included is shown in Fig. 11(c). It is dominated by the set of four crescent-shaped focusing structures B. Figure 11(d) shows the corresponding (innermost) sheet of the slowness surface. The oval, shaded areas are regions of negative Gaussian curvature. The parabolic lines bounding these regions map onto the crescent caustics B. As pointed out earlier, the fast phonon branch cannot display caustics when the elastic constants are unstiffened. These crescent caustics only come about because of the very large electromechanical coupling in Rochelle salt.

Another orthorhombic crystal which has fast phonon branch caustics is $Ba_2NaNb_5O_{15}$ (class $mm2$). Figure 12 shows the $\phi=0°$ section through the slowness surface of this material ($K_{33}=0.70$). There is a pronounced indentation centered on the [001] direction which leads to strong focusing in the region of this axis. Interestingly, although there are points of conical degeneracy between the outer two sheets, and therefore necessarily ST caustics, the overall intensity of the transverse focusing structures is much less than that of the L caustics.

$LiGaO_2$ and Li_2GeO_3 are two other orthorhombic crystals with large electromechanical coupling. Figure 13 shows the ST and FT focusing pattern of $LiGaO_2$ (class $mm2$), taking account of this coupling ($K_{33}=0.30$). Without stiffening of the elastic constants the caustics labeled A are absent, structures B and C are joined together, and structures C and D are separated. Li_2GeO_3 (class $mm2$) has a similar focusing pattern to $LiGaO_2$ and also comparable electromechanical coupling effects ($K_{33}=0.34$).

VII. NONLINEAR EFFECTS

The constitutive relations for piezoelectric media can be extended by incorporating terms which are quadratic or higher order in the electric and elastic variables. These nonlinear terms lead to various consequences. Phonon-phonon scattering and anharmonic decay are governed largely by the third- and higher-order elastic constants but are also influenced by the higher-order piezoelectric coupling coefficients, nonlinear permittivity coefficients, and various cross terms. These anharmonic processes all fall off rapidly with decreasing phonon frequency and thus can be rendered negligible by operating at sufficiently low temperatures.

Another consequence of these nonlinear terms is that the electric polarization $\mathbf{P}$ and electric displacement $\mathbf{D}$ do not average out to zero for a thermal distribution of phonons, and thus there is a pyroelectric effect. The most obvious terms to consider in this context are those involving the second-order piezoelectric stress coefficients $e_{rIJ}^{(2)}=\partial e_{rI}/\partial S_J$. As a rough estimate on this basis, the polarization of a medium is given by

$$P\sim e^{(2)}\langle S^2\rangle\sim e^{(2)}u/C\ , \tag{46}$$

where $e^{(2)}$ and C are suitable averages of the $e_{rIJ}^{(2)}$ and C_{IJ}, respectively, and u is the thermal energy density. One therefore expects the localized heat pulse in a phonon imaging experiment to be accompanied by a net dipole moment,

$$p\sim e^{(2)}U/C\ , \tag{47}$$

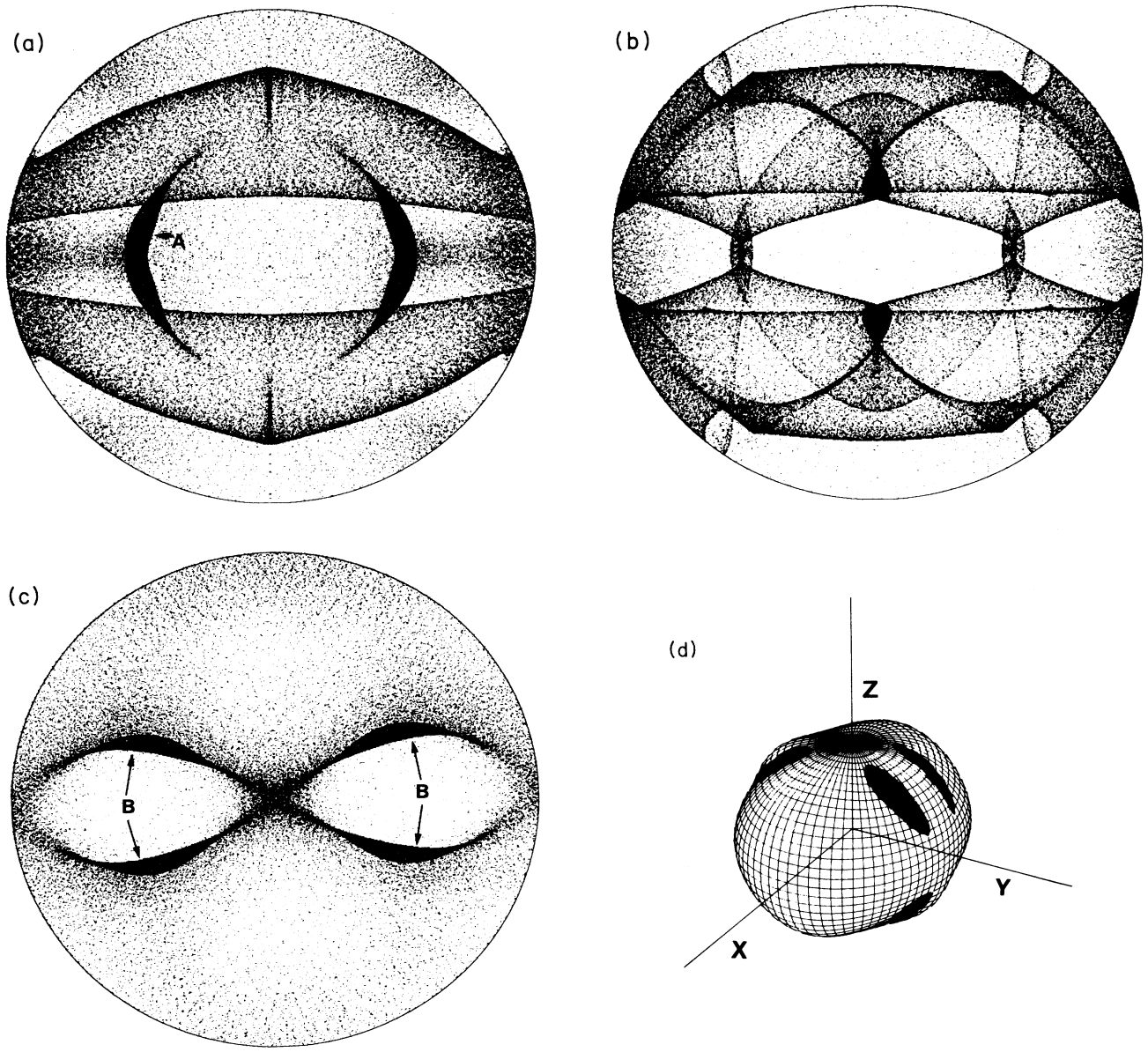

FIG. 11. Polar plot of the ST and FT phonon intensity of Rochelle salt (a) without piezoelectric effect, (b) with piezoelectric effect. (c) The L branch phonon intensity pattern, and (d) the L sheet of the slowness surface of Rochelle salt.

where U is the total energy contained in the pulse.

Surrounding this dipole there would be a long-range electric field,

$$E \sim \frac{p}{4\pi\epsilon r^3} \sim \frac{e^{(2)}U}{4\pi\epsilon r^3 C} , \tag{48}$$

which could conceivably produce a measurable signal in the bolometer. Taking $LiNbO_3$ as an example,[9] with $e^{(2)} = |e_{333}| = 21$ C/m^2, $C = C_{44} = 6\times 10^{10}$ N/m^2, and $\epsilon = \epsilon_{11} = 0.392\times 10^{-9}$ F/m, $U = 10^{-7}$ J, and $r = 10^{-2}$ m, one obtains $E = 0.007$ V/m. Assuming an active bolometer length of 10^{-4} m yields a signal of 1 μV. Since this signal depends on the integrated energy content of the heat pulse, it would remain essentially unchanged during the initial expansion of the heat pulse. Also **p** would have a specific orientation in any crystal, and the directional dependence of the bolometer signal would give an indication of this orientation. Equation (47) also implies that an individual phonon in a piezoelectric medium is endowed with a dipole moment $p \sim e^{(2)}\hbar\omega/C$. Perhaps the existence of this dipole could have observable consequences.

VIII. CONCLUSIONS

Using available data, we have shown that in a small but significant proportion of crystals piezoelectric stiffening of

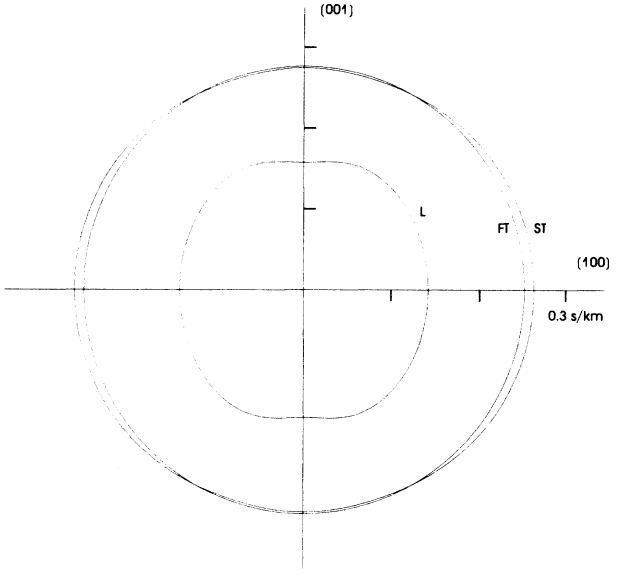

FIG. 12. The $\phi=0$ meridian section of the slowness surface of $Ba_2NaNb_5O_{15}$.

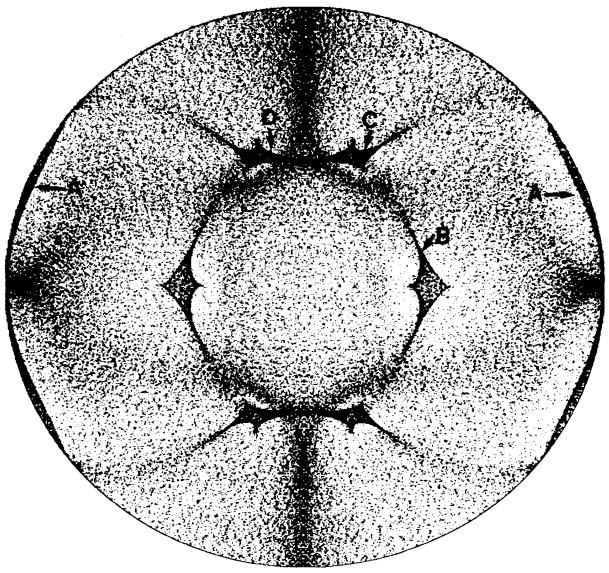

FIG. 13. Polar plot of the ST and FT phonon intensity of $LiGaO_2$ with piezoelectric stiffening.

the elastic constants has a pronounced influence on phonon focusing and other acoustic properties. On the whole, the effects of stiffening tend to be important only when the electromechanical coupling constants exceed ~ 0.1. For crystals which are nearly isotropic however, the piezoelectric effect is in direct competition with the residual elastic anisotropy and can play the dominant role even when the electromechanical coupling is much less than 0.1.

One of the important consequences of piezoelectric stiffening is that the equation for the slowness surface is raised in degree from 6 to 12. It thus becomes possible for the innermost sheet of this surface to possess regions of negative Gaussian curvature, and consequently for the fast phonon branch (normally longitudinal) to display focusing caustics. We have identified two crystals, Rochelle salt and $Ba_2NaNb_5O_{15}$, in which this phenomenon does indeed occur.

Our results underline the importance of taking into account the stiffening of elastic constants in the calculation of phonon focusing patterns. Although in many cases the results of stiffening are small, there are too many examples where the contrary is true for the effect to be ignored. The methods we have described for solving the Christoffel equations, and calculating group velocities and phonon focusing factors are sufficiently general to be applicable to crystals of any symmetry.

In conclusion, phonon imaging has an important role to play in the study of piezoelectric materials. In principle, it provides a means of measuring elastic constant ratios and electromechanical coupling constants and also of probing microscopic and macroscopic defects and other phonon scattering processes.[35] An interesting question that needs to be resolved is whether free-carrier shorting of the piezoelectric effect is operative and observable at thermal phonon frequencies. The strong electron-phonon coupling in piezoelectric semiconductors could make it difficult to achieve ballistic phonon propagation over experimentally significant distances. Another important issue for phonon imaging is that many of the more exotic piezoelectric materials have large unit cells or small elastic moduli and dispersive effects can therefore be expected in these materials at frequencies well below 1 THz.

ACKNOWLEDGMENTS

One of us (A.G.E.) would like to thank F.R.L. Schöning for illuminating discussions and M. J. R. Hoch for providing computer facilities.

[1]B. A. Auld, *Acoustic Fields and Waves in Solids* (Wiley, New York, 1973).

[2]S. Epstein, Phys. Rev. B 7, 1636 (1973).

[3]For reviews on phonon focusing and phonon imaging see G. A. Northrop and J. P. Wolfe, in *Nonequilibrium Phonon Dynamics,* edited by W. E. Bron (Plenum, New York, 1985), p. 165; H. J. Maris, in *Nonequilibrium Phonons in Non-metallic Crystals,* edited by W. Eisenmenger and A. A. Kaplyanskii (North-Holland, Amsterdam, 1986).

[4]A. K. McCurdy, H. J. Maris, and C. Elbaum, Phys. Rev. B 2, 4077 (1970); B. Taylor, H. J. Maris, and C. Elbaum, *ibid.* 3, 1462 (1971).

[5]W. I. F. David, J. Phys. C **16**, 2455 (1983).
[6]B. I. Klimenko, N. V. Perelomova, A. A. Blistanov, and V. S. Bondarenko, Kristallografiya **23**, 210 (1978) [Sov. Phys.—Crystallogr. **23**, 114 (1978); **26**, 213 (1980) [**26**, 118 (1981)].
[7]G. L. Koos and J. P. Wolfe, Phys. Rev. B **29**, 6015 (1984); **30**, 3470 (1984).
[8]J. F. Nye, *Physical Properties of Crystals* (Oxford University Press, London, 1957).
[9]W. R. Cook and H. Jaffe, in *Numerical Data and Functional Relationships in Science and Technology,* Vol. 11 of *Landolt-Börnstein, New Series,* edited by K. H. Hellwege (Springer, Berlin, 1979), Group III, pp. 287–470.
[10]M. J. P. Musgrave, *Crystal Acoustics* (Holden-Day, San Francisco, 1970).
[11]F. I. Fedorov, *Theory of Elastic Waves in Crystals* (Plenum, New York, 1968).
[12]R. F. S. Hearmon, in *Numerical Data and Functional Relationships in Science and Technology,* Ref. 9, Group III, pp. 1–244; *Numerical Data and Functional Relationships in Science and Technology,* Vol. 18 of *Landolt-Börnstein, New Series,* edited by K. H. Hellwege (Springer, Berlin, 1984), Group III, pp. 1–154.
[13]W. R. Cook, in *Numerical Data and Functional Relationships in Science and Technology,* Vol. 18 of *Landolt-Börnstein, New Series,* edited by K. H. Hellwege (Springer, Berlin, 1984), Group III, pp. 180–325.
[14]A. G. Every, Phys. Rev. B **22**, 1746 (1980).
[15]B. I. Klimenko, V. E. Lyamov, N. V. Perelomova, A. A. Blistanov, and V. S. Bondarenko, Kristallografiya **24**, 1268 (1979) [Sov. Phys.—Crystallogr. **24**, 725 (1979)].
[16]G. A. Northrop and J. P. Wolfe, Phys. Rev. B **22**, 6196 (1980).
[17]A. G. Every, G. L. Koos, and J. P. Wolfe, Phys. Rev. B **29**, 2190 (1984); A. G. Every, *ibid.* **33**, 2719 (1986).
[18]A. G. Every, J. Phys. C (to be published).
[19]J. C. Hensel and R. C. Dynes, Phys. Rev. Lett. **43**, 1033 (1979); P. Taborek and D. Goodstein, Phys. Rev. B **22**, 1550 (1980).
[20]H. J. Maris, J. Acoust. Soc. Am. **50**, 812 (1971).
[21]M. Lax and V. Narayanamurti, Phys. Rev. B **22**, 4876 (1980).
[22]A. G. Every, Phys. Rev. B **24**, 3456 (1981); A. G. Every and A. J. Stoddart, *ibid.* **32**, 1319 (1985).
[23]G. F. D. Duff, Philos. Trans. R. Soc. London **252**, 249 (1960).
[24]F. Rösch and O. Weis, Z. Phys. B **25**, 115 (1976).
[25]A. K. McCurdy, Phys. Rev. B **26**, 6971 (1982).
[26]D. C. Hurley and J. P. Wolfe, Phys. Rev. B **32**, 2568 (1985).
[27]V. I. Al'shits and A. L. Shuvalov, Kristallografiya **29**, 629 (1984) [Sov. Phys.—Crystallogr. **29**, 373 (1984)].
[28]G. Kanellis, W. Kress, and H. Bilz, Phys. Rev. B **33**, 8724 (1986).
[29]A. K. McCurdy, Phys. Rev. B **9**, 466 (1974).
[30]A. G. Every, Phys. Rev. B **34**, 2852 (1986).
[31]F. Rösch and O. Weis, Z. Phys. B **25**, 101 (1976).
[32]C. G. Winternheimer and A. K. McCurdy, Phys. Rev. B **18**, 6576 (1978).
[33]D. C. Hurley, J. P. Wolfe, and K. A. McCarthy, Phys. Rev. B **33**, 4189 (1986).
[34]D. Armbruster and G. Dangelmayr, Z. Phys. B **52**, 87 (1983); M. V. Berry, Adv. Phys. **25**, 1 (1976).
[35]See, for example, G. A. Northrop, E. J. Cotts, A. C. Anderson, and J. P. Wolfe, Phys. Rev. B **27**, 6395 (1983); R. P. Huebener and W. Metzger, Scanning Electron Microsc. **II**, 617 (1985).

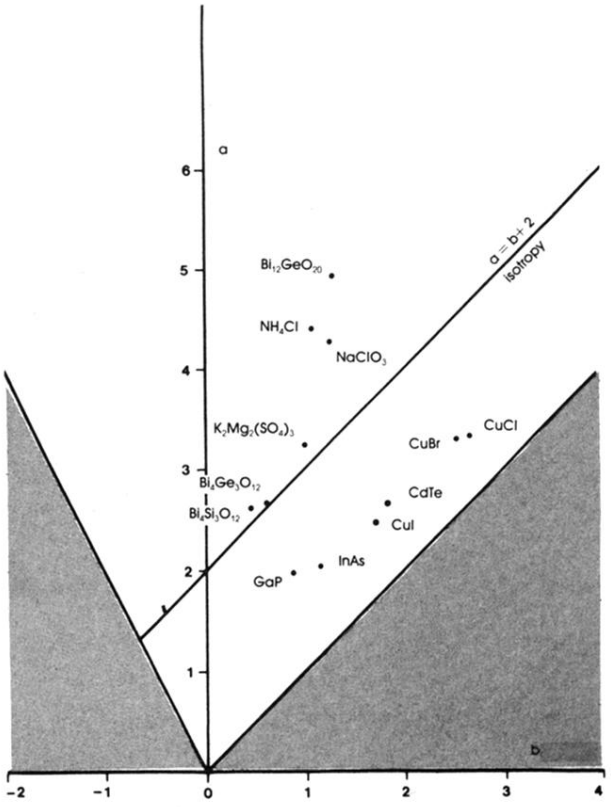

FIG. 2. Elastic constant ratios of the more strongly piezoelectric cubic crystals ($a = C_{11}/C_{44}$ and $b = C_{12}/C_{44}$).